International Journal of Minerals, Metallurgy and Materials
Volume 27, Number 3, March 2020, Page 340
https://doi.org/10.1007/s12613-019-1881-y

Effect of austempering time on microstructure and properties of a low-carbon bainite steel

Man Liu, Guang Xu, Jun-yu Tian, Qing Yuan, and Xin Chen

The State Key Laboratory of Refractories and Metallurgy, Wuhan University of Science and Technology, Wuhan 430081, China

(Received: 19 May 2019; revised: 3 July 2019; accepted: 8 July 2019)

Abstract: The effect of austempering time after the bainitic transformation on the microstructure and property in a low-carbon bainite steel was investigated by metallography and dilatometry. The results showed that by prolonging the austempering time after the bainite transformation, the amount of large-size martensite/austenite islands decreased, but no significant change of the amount and morphology of bainite were observed. In addition, more austenite with a high carbon content was retained by prolonging the holding time at the bainite transformation temperature. Moreover, with a longer holding time, the elongation was improved at the expense of a small decrease in tensile strength. Finally, the Avrami equation $B_{RF} = 1 - \exp(-0.0499 \times t^{0.7616})$ for bainite reaction at 350°C was obtained for the tested steel. The work provided a reference for tailoring the properties of low-carbon steels.

Keywords: austempering time; retained austenite; martensite/austenite island; low-carbon bainite; transformation kinetics

1. Introduction

The bainite reaction normally occurs at intermediate temperature and is associated with more controversy than any other transformations in the field of physical metallurgy [1−7]. Bainite transformation is affected by many factors such as alloying elements [8−14], heat treatment parameters [15−20], and deformation conditions [21−25]. For example, the addition of niobium has been found to retard bainitic transformation, while molybdenum addition effectively promoted bainitic reaction in low-carbon bainite steels [11]. A finer bainite microstructure was obtained in the specimen austempered below Martensite start temperature (M_s) compared with the specimen held above M_s [17]. Huang *et al.* [18] obtained better ductility and increased strength and elongation in low-carbon steels subjected to B-QP (bainitic isothermal transformation plus quenching and partitioning) treatment compared to those subjected to Q-P (quenching and partitioning) treatment. Hu *et al.* [21] revealed the impacts of deformation temperature and strain on bainite precipitation. They claimed that the degree of bainite growth retardation increased more quickly with strain, while the degree of bainite reaction promotion by nucleation increased slowly. These studies consider only one isothermal time after bainite transformation. A few studies focused on the effect of prolonging austempering time after bainite reaction on the microstructure and mechanical properties. For example, Morales-Rivas *et al.* [26] investigated the tensile response of the composite microstructure of high-carbon, high-silicon steels and clarified that prolonging the holding time at bainite transformation temperature resulted in higher ductility, a considerable coarsening of the bainite plates and retained austenite (RA). However, only few studies have addressed the effect of prolonged austempering time after transformation on the microstructure and properties of low-carbon bainite steels. Therefore, in the present study, longer holding times after the bainitic transformation were designed to clarify the effect of prolonged austempering time on the microstructure and properties of low-carbon bainite steels. The work provided a reference for tailoring the properties of low-carbon bainite steels.

2. Experimental

The tested steel with a chemical composition (Table 1) was refined by a laboratory-scale vacuum furnace. Molyb-

Corresponding author: Guang Xu E-mail: xuguang@wust.edu.cn

denum addition can accelerate bainite transformation. The ingots were hot-rolled and were then air-cooled to ambient temperature. Specimens were machined to ϕ 8.0 mm × 12.0 mm cylinders for thermomechanical simulation tests. According to the time-temperature transformation (TTT) curve of the tested steel (Fig. 1(a)) plotted using JMatPro 7.0 [14], the temperature range of the bainite reaction was between 330.6 and 503.1°C. It is known that a high transformation temperature of bainite reaction led to coarse grains and poor mechanical properties [27]. Hence, 350°C, slightly above M_s, was chosen as the bainite transformation temperature to obtain finer lathlike bainite ferrite.

Table 1. Chemical composition of the tested steel wt%

C	Si	Mn	Mo	Fe
0.220	2.012	2.197	0.218	Bal.

Thermal simulation experiments were conducted on a Gleeble 3500 simulator according to the procedure in Fig. 2. Specimens were austenized for 15 min at 1000°C and then isothermally transformed at 350°C for different times before air-cooling to ambient temperature. According to the continuous cooling transformation (CCT) curve in Fig. 1(b), a relatively larger cooling rate of 20°C/s is needed to avoid high-temperature proeutectoid ferrite or pearlite transformation [28]. At 350°C, the holding time of the specimens was 3, 5, 30, and 60 min, and these routes were termed as A-3, A-5, A-30, and A-60, respectively. Finally, all specimens were cooled to ambient temperature at 5°C/s.

All specimens were prepared for microstructure observation by mechanical grinding and polishing before being etched with 4vol% nital. A Nova400 Nano field-emission scanning electron microscope (SEM) was utilized to observe the microstructure, and an acceleration voltage of 20 kV was selected. Quantitative X-ray diffraction (XRD) analysis was carried out to measure the amount and carbon content of the RA. The amount of austenite and the carbon concentration in the RA were calculated using the following equations:

$$V_i = \frac{1}{1 + G(I_\alpha / I_\gamma)} \tag{1}$$

$$C_\gamma = \left(\frac{\lambda \sqrt{h^2 + k^2 + l^2}}{2 \sin\theta} - 3.578 \right) / 0.033 \tag{2}$$

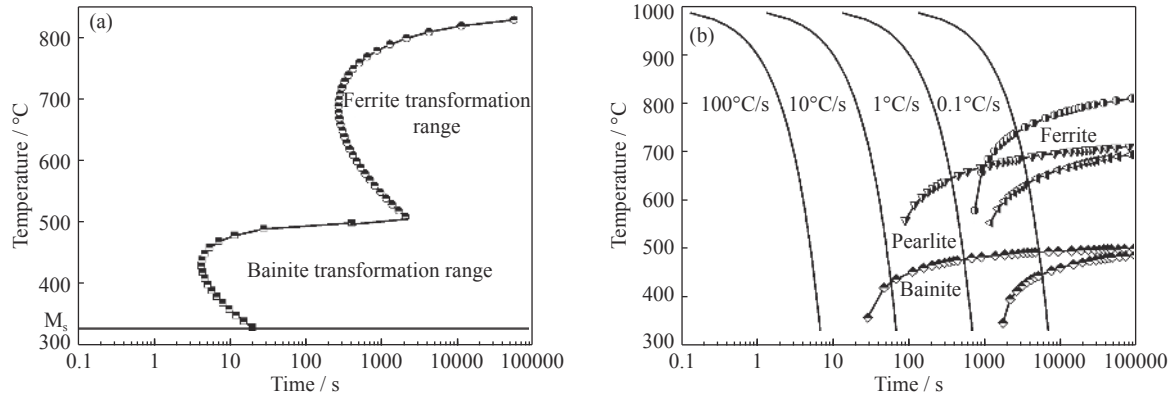

Fig. 1. Time–temperature transformation (a) and the continuous cooling transformation (b) curves of the tested steel.

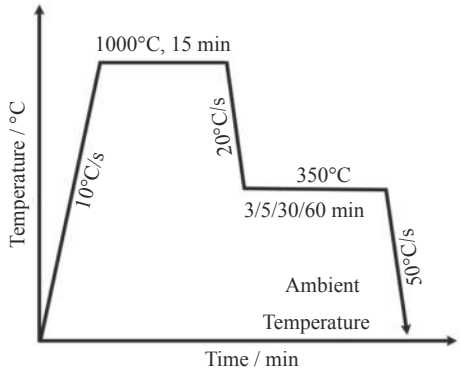

Fig. 2. Illustration of the experimental procedure.

where V_i is the amount of austenite for each peak, I_α and I_γ represent the integrated intensities of ferrite (bcc) and austenite (fcc) peaks, respectively, and the G value for each peak is defined in Ref. [29]. Moreover, θ are the angle of (200), (220), and (311) diffraction peaks, and λ (λ = 0.178892 nm) is the wavelength of X-ray. The volume fraction of each phase in microstructure was calculated using Image-Pro Plus. In addition, tensile tests were carried out on a UTM-5305 electronic universal tensile tester at room temperature, and the strain rate was 4×10^{-3} s^{-1}. To improve the accuracy, three tensile specimens of each isothermal time were prepared, and the average value of the three tensile tests was obtained as the final results.

3. Results and discussion

3.1. Dilatation

Fig. 3 illustrates the dilatation curves of specimens and the relative fraction of bainite. The fluctuation of isothermal transformation temperature was controlled within the range of ±0.5°C. The dilatation amount in Fig. 3(a) represents the volume fractions of bainitic during the isothermal transformation period of different specimens. The bainitic transformation at 350°C was observed to terminate at about 7 min. The relative volume fraction of bainite (B_{RF}) was equal to the relative dilatation strain (d_i/d_{max}) during the bainitic transformation. According to the instantaneous expansion amount (d_i) and the maximum expansion amount (d_{max}) during the bainitic transformation, the relative expansion strain at different time was calculated; thus, the curve of B_{RF} with time was obtained (Fig. 3(b)). The kinetic curve was fitted by Avrami kinetic Eq. (3), and the result is illustrated in Fig. 3 (solid line).

$$B_{RF} = 1 - \exp(-bt^n) \quad (3)$$

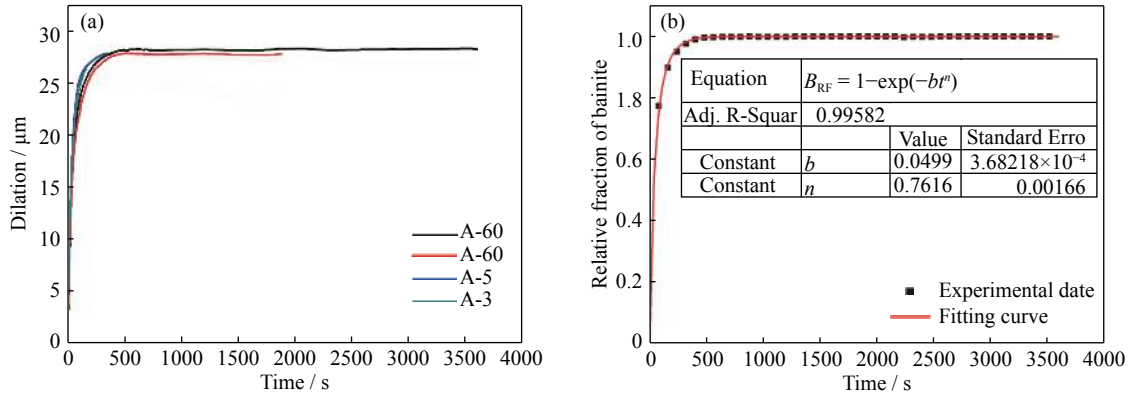

Fig. 3. Dilatation curves of bainite transformation for different specimens (a) and the curve of the relative fraction of bainite (B_{RF}) with time (b).

where t is the transformation time, b is the kinetic parameter, and n is the equation index. The Avrami equation $B_{RF} = 1 - \exp(-0.0499 \times t^{0.7616})$ for bainite transformation was obtained for the tested low-carbon bainite steel based on the dilatation data. The fitting results showed that Avrami equation well described the bainitic reaction kinetics of the tested low-carbon bainite steel.

3.2. Microstructure

Fig. 4 depicts the microstructure of specimens after different holding time at 350°C obtained by scanning electron microscopy (SEM). As observed, the microstructure of the specimens contained lathlike bainite ferrite (BF), film-like RA, and martensite with/without austenite. Martensite/austenite (M/A) islands contained martensite and austenite, whereas martensite without austenite presented a large blocky morphology, which was formed during cooling to ambient temperature. Cementite precipitates can be prevented due to the addition of ~1.5wt% silicon [30−33]. Thus, no cementite precipitates were formed in the microstructure. The amount of large-size M/A was observed to decrease with increasing the holding time at 350°C, but the morphology of bainite showed few differences among A-5, A-30, and A-60

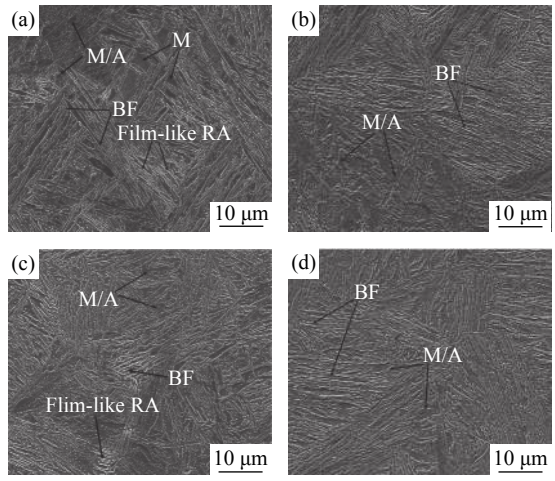

Fig. 4. SEM images of the specimens after different holding times at 350°C: (a) 3 min; (b) 5 min; (c) 30 min; (d) 60 min.

specimens. The amount change of large-size M/A may be attributed to the carbon redistribution and the change in the chemical stability of austenite. Except for the specimen held at 350°C for 3 min (i.e., A-3), bainite transformation proceeded in other specimens, and compared with A-3, the residual austenite in the other specimens contained a high carbon content due to the rejection of carbon from bainite to the

adjacent austenite, resulting in the high stability of the residual austenite. Thus, blocky martensite was difficult to form in A-5, A-30, and A-60 specimens. On the other hand, prolonging the holding time after the bainitic reaction at 350°C resulted in more carbon content in the residual austenite; thus the blocky large-size M/A was hard to form. Therefore, the amount of large-size M/A decreased with the increase of holding time at 350°C.

Based on several micrographs, the amounts of bainite were calculated by Image-Pro Plus 6.0. The lathlike bainite was different from the blocky martensite in morphology, and in the SEM micrographs, dark bainite was distinguished from white RA by color. Fig. 5 shows an example for calculating the bainite amount. The darker regions consisted of bainite and M/A (Fig. 5(a)). First, the darker areas were automatically colored in red using Image-Pro Plus (Fig. 5(b)). The area percentage of red regions could be automatically calculated by the software, and the result is termed as S_1. Then, the darker blocky regions were M/A islands, which should be subtracted from the red regions. The darker blocky regions were carefully and manually marked, as shown in Fig. 5(c). The percentage of blocky regions (labeled as S_2) was measured by Image-Pro Plus 6.0. Third, the remaining part (labeled as S_3) was obtained by $S_3 = S_1 - S_2$, which was the amount of bainite. In this example, S_1 and S_2 were calculated to be 67.68% and 4.67%, respectively, so that S_3 was 63.01%. Therefore, the bainite amount in A-3 specimen was measured to be (63.01±2.32)%. Similarly, the bainite amounts in A-5, A-30, and A-60 specimens were determined to be (69.39±3.24)%, (70.08±3.65)%, and (70.42±3.74)%, respectively. To increase the accuracy of statistical results, several typical SEM micrographs of each specimen were calculated, and the average value was obtained as the final result. This indicated that the bainite amount increased with the increase of holding time from 3 min to 5 min, but no significant change in bainite amounts were observed in A-5, A-30, and A-60 specimens.

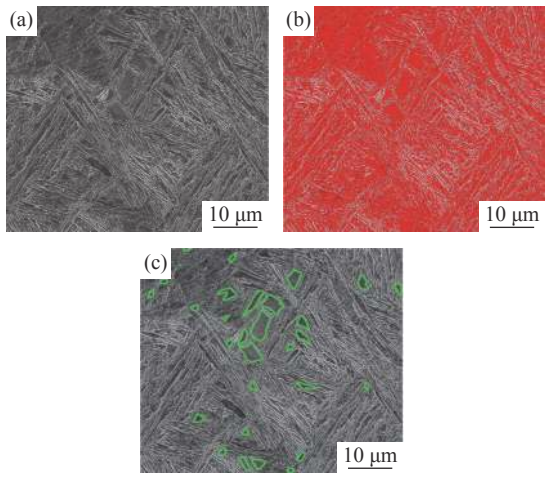

Fig. 5. Example showing the method of calculating the volume fraction of bainite: (a) the original micrograph; (b) the darker areas in (a) (shown in red); (c) the darker blocky regions in (b) (manually marked).

3.3. XRD experiments

Fig. 6 illustrates the diffraction patterns of specimens obtained by XRD experiments. The angles of diffraction peaks and the integrated intensities were computed by the High Score Plus software. The amount and carbon content of RA were calculated according to Eqs. (1) and (2), respectively, and the average values of V_i and C_γ were obtained as the final results. XRD measurements represented an average value of the carbon content in RA. It should be pointed out that a great difference existed between the carbon contents of the blocky and thin-film RA. The carbon enrichment was high in the film RA between the bainite plates. The amount and carbon content of RA are given in Fig. 7. The figure displayed that the amount and carbon content of RA increased with the increase of holding time at 350°C. With longer austempering time, the blocky RA decreased (Fig. 3), while the RA amount increased, meaning more film-like RA was presented in the microstructure. Only carbon diffusion was considered here because the activity of carbon is much greater than Mn and Si at 350°C. With the extension of the isothermal time, bainite transformation did not further proceed; thus, there should exist other sources for more carbon in A-30 and A-60 specimens. It is known that after bainite reaction, some carbon atoms are trapped at dislocations and other defects [34−38]. The isothermal holding after the transformation provided a condition for the diffusion of carbon atoms to adjacent austenite. With the extension of the holding time, the recovery of dislocations resulted in a release of

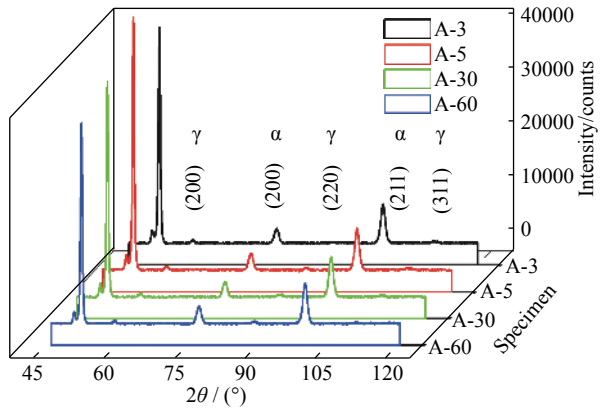

Fig. 6. Diffraction peaks of specimens.

the carbon. Hence, the residual austenite was further carbon-enriched with prolonged isothermal time, increasing the chemical stability of untransformed austenite. Finally, more austenite was retained at ambient temperature, and the carbon content in the RA was high. Huang *et al*. [19] studied the effect of quenching-long partitioning treatment on the microstructure and properties of a low-carbon alloyed steel. They reported that impact toughness at room temperature was significantly improved by quenching-long partitioning treatment due to more carbon partitioning and stress relief. The main differences between their study and the present investigation are as follows: First, the chemical compositions in the two studies were different, and Ref. [19] considered more alloying elements. Second, the investigation purpose was different. Ref. [19] focused on the effect of partitioning time on impact toughness in a Q&P steel, while the present study investigated the effect of prolonged isothermal holding time after bainitic transformation on the RA and properties. Third, in the reference, the partitioning temperature was below M_s, whereas the isothermal temperature in this study exceeded M_s.

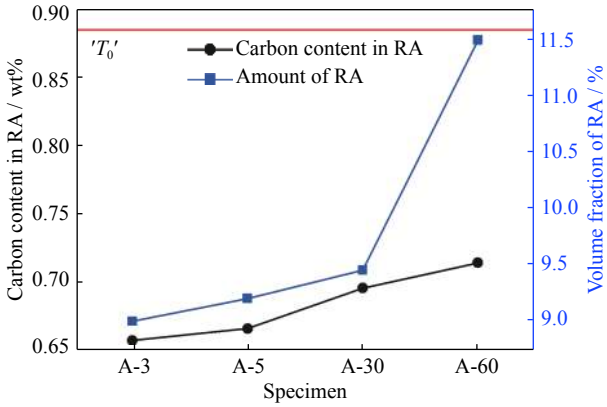

Fig. 7. Carbon content and volume fraction of RA with different specimens.

Using the T_0 theory, the maximum carbon content in the RA after the bainitic transformation at 350°C was calculated to be 0.885wt%, which is plotted in Fig. 7. The T_0 curve represented the collection of the points of maximum carbon content in austenite at different temperatures. Thus, the bainite transformation ceased when the carbon content in austenite reached the limit at a given temperature. In addition, stored energy caused by bainitic transformation moved the T_0 curve leftward, resulting in the carbon content in austenite being less than the maximum carbon content by T_0. The less carbon content in austenite resulted in the early finishing of bainitic transformation. Therefore, both the carbon content and stored energy determined the incompletion of bainitic transformation. The carbon content in the RA of the four specimens were lower than the calculated theoretical value of T_0, indicating that the bainite precipitation had the characteristic of incomplete reaction [39].

3.4. Mechanical properties

Fig. 8 shows the engineering strain–stress curves of different specimens, and the tensile results are given in Table 2. The tensile behaviors presented a clear transformation–induced plasticity (TRIP) effect. The amount and stability of the RA are known to be of critical importance to the TRIP effect. The stability was affected by the amount, carbon content, grain size, and morphology of RA. Prolonging the austempering time resulted in an increase of the amount of RA and its carbon content, as well as the increase of film-like RA, leading to a more pronounced TRIP effect. The elongation increased at the expense of a small decrease in tensile strength by prolonging the austempering time after the bainitic transformation, which corresponded to the results of XRD experiment.

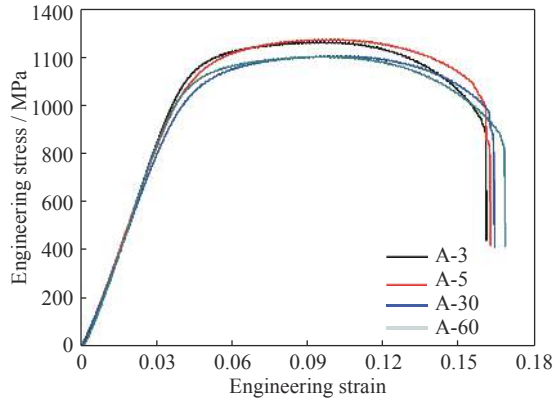

Fig. 8. Engineering strain–stress curves of different specimens.

Table 2. Mechanical properties of different specimens

Specimen	Tensile strength / MPa	Yield strength / MPa	Elongation / %
A-3	1267 ± 33	1090 ± 20	16.00 ± 0.10
A-5	1278 ± 35	1109 ± 36	16.21 ± 0.12
A-30	1215 ± 21	1126 ± 38	16.36 ± 0.15
A-60	1204 ± 17	1126 ± 41	16.88 ± 0.16

4. Conclusions

The effects of the prolonged austempering time after the bainitic reaction on the microstructure and mechanical properties of a low-carbon bainite steel were investigated by metallography, dilatometry, XRD, and tensile tests. The results showed that by prolonging the austempering time after

the bainitic transformation, the amount of large-size martensite/austenite island decreased, but no significant change in amount and morphology of bainite was observed. In addition, more austenite with high carbon content was retained. Moreover, prolonging the austempering time resulted in an increase of the amount of RA and its carbon content, as well as the increase of film-like RA, leading to a more pronounced TRIP effect. Therefore, the elongation was improved at the expense of a small decrease in tensile strength.

Acknowledgements

The authors gratefully acknowledge the financial supports from the National Natural Science Foundation of China (NSFC) (Nos. 51874216 and 51704217) and the Major Projects of Technology Innovation of Hubei Province, China (No. 2017AAA116).

References

[1] H.K.D.H. Bhadeshia, *Bainite in Steels*, 2nd ed., IOM Communications Ltd. London, 2001.

[2] H.I. Aaronson, T. Furuhara, J.M. Rigsbee, W.T. Reynolds, and J.M. Howe, Crystallographic and mechanistic aspects of growth by shear and by diffusional processes, *Metall. Trans. A*, 21(1990), No. 9, p. 2369.

[3] Z. Lawrynowicz and A. Barbacki, Features of bainite transformation in steels, *Adv. Mater. Sci.*, 2(2002), No. 1, p. 5.

[4] Y. Ohmori, Bainite transformations in extremely low carbon steels, *ISIJ Int.*, 35(1995), No. 8, p. 962.

[5] H.K.D.H. Bhadeshia, The bainite transformation: Unresolved issues, *Mater. Sci. Eng. A*, 273-275(1999), p. 58.

[6] M. Hillert, Paradigm shift for bainite, *Scripta Mater.*, 47(2002), No. 3, p. 175.

[7] A. Borgenstam, M. Hillert, and J. Ågren, Metallographic evidence of carbon diffusion in the growth of bainite, *Acta Mater.*, 57(2009), No. 11, p. 3242.

[8] J.Y. Tian, G. Xu, Z.Y. Jiang, X.L. Wan, H.J Hu, and Q. Yuan, Transformation behavior and properties of carbide-free bainite steels with different Si contents, *Steel Res. Int.*, 90(2019), No. 3, art No. 1800474.

[9] Z.S. Yao, G. Xu, H.J. Hu, Q. Yuan, J.Y. Tian, and M.X. Zhou, Effect of Ni and Cr addition on transformation and properties of low-carbon bainitic steels, *Trans. Indian Inst. Met.*, 72(2019), No. 5, p. 1167.

[10] J.Y. Tian, G. Xu, M.X. Zhou, H.J. Hu, and Z.L. Xue, Effects of Al addition on bainite transformation and properties of high-strength carbide-free bainitic steels, *J. Iron Steel Res. Int.*, 26(2019), No. 8, p. 846.

[11] H.J. Hu, G. Xu, L. Wang, Z.L. Xue, Y.L. Zhang, and G.H. Liu, The effects of Nb and Mo addition on transformation and properties in low carbon bainitic steels, *Mater. Des.*, 84(2015), p. 95.

[12] X.D. Wang, B.X. Huang, L. Wang, and Y.H. Rong, Microstructure and mechanical properties of microalloyed high-strength transformation–induced plasticity steels, *Metall. Mater. Trans. A*, 39(2008), No. 1, p. 1.

[13] T. Heller and A. Nuss, Effect of alloying elements on microstructure and mechanical properties of hot rolled multiphase steels, *Ironmaking Steelmaking*, 32(2005), No. 4, p. 303.

[14] J.Y. Tian, G. Xu, M.X. Zhou, H.J. Hu, and X.L. Wan, The Effects of Cr and Al addition on transformation and properties in low-carbon bainitic steels, *Metals*, 7(2017), No. 2, p. 40.

[15] Z.N. Yang, C.H. Chu, F. Jiang, Y.M. Qin, X.Y. Long, S.L. Wang, D. Chen, and F.C. Zhang, Accelerating nano-bainite transformation based on a new constructed microstructural predicting model, *Mater. Sci. Eng. A*, 748(2019), p. 16.

[16] G.H. Gao, H. Zhang, X.L. Gui, P. Luo, Z.L. Tan, and B.Z. Bai, Enhanced ductility and toughness in an ultrahigh-strength Mn–Si–Cr–C steel: the great potential of ultrafine filmy retained austenite, *Acta Mater.*, 76(2014), p. 425.

[17] J.Y. Tian, G. Xu, M.X. Zhou, and H.J. Hu, Refined bainite microstructure and mechanical properties of a high-strength low-carbon bainitic steel treated by austempering below and above Ms, *Steel Res. Int.*, 89(2018), No. 4, art No. 1700469.

[18] Y.Y. Huang, Q.G. Li, X.F. Huang, and W.G. Huang, Effect of bainitic isothermal transformation plus Q&P process on the microstructure and mechanical properties of 0.2C bainitic steel, *Mater. Sci. Eng. A*, 678(2016), p. 339.

[19] X.F Huang, W.L. Liu, Y.Y. Huang, H. Chen, and W.G. Huang, Effect of a quenching-long partitioning treatment on the microstructure and mechanical properties of a 0.2C% bainitic steel, *J. Mater. Process. Technol.*, 222(2015), p. 181.

[20] Q.G. Li, X.F. Huang, and W.G. Huang, Fatigue property and microstructure deformation behavior of multiphase microstructure in a medium-carbon bainite steel under rolling contact condition, *Int. J. Fatigue*, 125(2019), p. 381.

[21] H.J. Hu, G. Xu, M.X. Zhou, and Q. Yuan, New insights to the promoted bainitic transformation in prior deformed austenite in a Fe−C−Mn−Si alloy, *Met. Mater. Int.*, 23(2017), No. 2, p. 233.

[22] W. Gong, Y. Tomota, Y. Adachi, A.M. Paradowska, J.F. Kelleher, and S.Y. Zhang, Effects of ausforming temperature on bainite transformation, microstructure and variant selection in nanobainite steel, *Acta Mater.*, 61(2013), No. 11, p. 4142.

[23] J.G. He, A.M. Zhao, C. Zhi, and H.L. Fan, Acceleration of nanobainite transformation by multi-step ausforming process, *Scripta Mater.*, 107(2015), p. 71.

[24] H.J. Hu, G. Xu, F.Q. Dai, J.Y. Tian, and G.H. Chen, Critical ausforming temperature to promote isothermal bainitic transformation in prior-deformed austenite, *Mater. Sci. Technol.*, 35(2019), No. 4, p. 420.

[25] H. Zou, H.J. Hu, G. Xu, Z.L. Xiong, and F.Q. Dai, Combined effects of deformation and undercooling on isothermal bainitic transformation in an Fe−C−Mn−Si alloy, *Metals*,

9(2019), No. 2, p. 138.
[26] L. Morales-Rivas, H.W. Yen, B.M. Huang, M. Kuntz, F.G. Caballero, J.R. Yang, and C. Garcia-Mateo, Tensile response of two nanoscale bainite composite-like structures, *JOM*, 67(2015), No. 10, p. 2223.
[27] L.J. Zhao, L.H. Qian, J.Y. Meng, Z. Qian, and F.C. Zhang, Below-Ms austempering to obtain refined bainitic structure and enhanced mechanical properties in low-C high-Si/Al steels, *Scripta Mater.*, 112(2016), p. 96.
[28] Z.W. Hu, G. Xu, C. Zhang, and H.J. Hu, Research on continuous cooling transformation curve of a C−Si−Mn steel, *Appl. Mech. Mater.*, 556-562(2014), p. 404.
[29] C.Y. Wang, J. Shi, W.Q. Cao, and H. Dong, Characterization of microstructure obtained by quenching and partitioning process in low alloy martensitic steel, *Mater. Sci. Eng. A*, 527(2010), No. 15, p. 3442.
[30] L.I. Lin, B.C.D. Cooman, P. Wollants, H.E. Yanlin, and X. Zhou, Effect of aluminum and silicon on transformation induced plasticity of the TRIP steel, *Mater. Sci. Technol.*, 20(2004), No. 2, p. 135.
[31] W.C. Jeong, Effect of silicon content and annealing temperature on formation of retained austenite and mechanical properties in multi-phase steels, *Met. Mater. Int.*, 9(2003), No. 2, p. 179.
[32] K.I. Sugimoto, Fracture strength and toughness of ultra high strength TRIP aided steels, *Mater. Sci. Technol.*, 25(2009), No. 9, p. 1108.
[33] P. Jacques, E. Girault, T. Catlin, N. Geerlofs, T. Kop, S. van der Zwaag, and F. Delannay, Bainite transformation of low carbon Mn−Si TRIP-assisted multiphase steels: influence of silicon content on cementite precipitation and austenite retention, *Mater. Sci. Eng. A*, 273-275(1999), p. 475.
[34] M. Peet, S.S. Babu, M.K. Miller, and H.K.D.H. Bhadeshia, Three-dimensional atom probe analysis of carbon distribution in low-temperature bainite, *Scripta Mater.*, 50(2004), No. 10, p. 1277.
[35] E.V. Pereloma, I.B. Timokhina, M.K. Miller, and P.D. Hodgson, Three-dimensional atom probe analysis of solute distribution in thermomechanically processed trip steels, *Acta Mater.*, 55(2007), No. 8, p. 2587.
[36] F.G. Caballero, M.K. Miller, A.J. Clarke, and C. Garcia-Mateo, Examination of carbon partitioning into austenite during tempering of bainite, *Scripta Mater.*, 63(2010), No. 4, p. 442.
[37] I.B. Timokhina, X.Y. Xiong, H. Beladi, S. Mukherjee, and P.D. Hodgson, Three-dimensional atomic scale analysis of microstructures formed in high strength steels, *Mater. Sci. Technol.*, 27(2011), No. 4, p. 739.
[38] S.N. Prasad, A. Saxena, M.M.S. Sodhi, and P.N. Tripathi, Influence of different heat treatment parameters on microstructure and mechanical properties of C−Mn strapping quality steels, *Mater. Sci. Eng. A*, 476(2008), No. 1-2, p. 126.
[39] F.G. Caballero, C. Garcia-Mateo, M.J. Santofimia, M.K. Miller, and C.G.D. Andrés, New experimental evidence on the incomplete transformation phenomenon in steel, *Acta Mater.*, 57(2009), No. 1, p. 8.